energies

MDPI

Article

An Experimental and Numerical Study on Charged 21700 Lithium-Ion Battery Cells under Dynamic and High Mechanical Loads

Marian Bulla [1,*], Christopher Schmandt [2], Stefan Kolling [2], Thomas Kisters [3] and Elham Sahraei [4,5]

[1] Altair Engineering GmbH, Josef-Lammerting-Allee 10, 50933 Cologne, Germany
[2] Institute of Mechanics and Materials, Technische Hochschule Mittelhessen, Wiesenstr. 14, 35390 Giessen, Germany
[3] Fraunhofer Institute for High-Speed Dynamics, Ernst-Mach-Institut, Ernst-Zermelo-Straße 4, 79104 Freiburg, Germany
[4] Electric Vehicle Safety Lab (EVSL), Temple University, Philadelphia, PA 19122, USA
[5] Massachusetts Institute of Technology, Cambridge, MA 02139, USA
* Correspondence: bulla@altair.com; Tel.: +49-160-96367668

Abstract: The need for higher capacity battery cells has increased significantly during the past years. Therefore, the subject of this study is to investigate the behavior of high performance 21700 Lithium-Ion cylindric battery cells under several abuse conditions, represented by high mechanical loads with different velocities and states of charge (SoC), and to develop a finite element analysis (FEA) model, using the OpenRadioss' explicit solver capabilities. The present study is focused on the investigation of the behavior of these cells under high mechanical loads with different loading velocities and different states of charge. The aim of the study is to provide a tool to predict the point of an internal short circuit in FEA, with a very good approximation. Experiments were completed using a hydraulic flat-compression test, set up at four different states of charge, 40%, 60%, 80% and 100%, and three different loading velocities of 10 mms^{-1}, 100 mms^{-1} and 1000 mms^{-1}. A homogenized FEA model is developed to predict the internal damage of the separator, which can lead to a short circuit with a possible thermal runaway under abusive load conditions. The present model, in combination with well identified material and fracture parameters, succeeded in the prediction of the mechanical behavior at various states of charge and mechanical loading conditions; it can also be used for further crashworthiness analysis within a full-car FEA model. This accurate cell model will be the first building block to optimize the protective structures of batteries in electric vehicles, and reduce their weight through a deeper understanding of their overall behavior during the different crash cases.

Keywords: 21700 Li-Ion battery; state of charge; orthotropy; material model; failure model; finite element model; OpenRadioss; safety; crashworthiness; battery safety; internal short circuit

check for updates

Citation: Bulla, M.; Schmandt, C.; Kolling, S.; Kisters, T.; Sahraei, E. An Experimental and Numerical Study on Charged 21700 Lithium-Ion Battery Cells under Dynamic and High Mechanical Loads. *Energies* **2023**, *16*, 211. https://doi.org/10.3390/en16010211

Academic Editor: Carlos Miguel Costa

Received: 30 November 2022
Revised: 20 December 2022
Accepted: 21 December 2022
Published: 25 December 2022

Copyright: © 2022 by the authors. Licensee MDPI, Basel, Switzerland. This article is an open access article distributed under the terms and conditions of the Creative Commons Attribution (CC BY) license (https://creativecommons.org/licenses/by/4.0/).

1. Introduction

Driven by the need to limit global warming and reduce the usage of fossil energy sources such as oil and gas, huge efforts are being made to increase the use of renewable energy sources to produce electrical energy. Due to the non-continuous availability of most renewable energy sources, such as photovoltaic or wind energy, it is necessary to be able to store the electrical energy produced by these energy sources [1]. The use of lithium-ion batteries has proven to be a very effective method of storing the electrical energy obtained in this way. This technology has been successfully used in the automotive industry and in consumer electronics for many years. Li-ion batteries offer the advantage of a high energy density and a low self-discharge rate [2]. Due to the rapid increase in the usage of this storage technology, the demand for an increase in the storage capacity of these batteries is also rising. The widely used 18650 Li-ion batteries in the automotive industry is increasingly

being substituted for batteries with a higher capacity. As a possible alternative to the 18650 Li-Ion batteries, the use of the higher capacity 21700 Li-Ion batteries, which have been available since 2016, in consumer goods, e-bikes and the automotive industry, has become established [3]. These batteries are the subject of the present study. There are other types of batteries [4] that will not be discussed further within this study, such as nickel–cadmium, nickel-metal hydride, lithium-ion polymer, and others. Canals Casals et al. [5] underline the need for higher capacity batteries, especially in electric vehicles. There are different shapes and sizes of Li-Ion batteries. The designation of form factor for cylindrical batteries includes using 4 or 5 digits as the cell type, where the first two digits describe the nominal diameter, and the following two digits describe the nominal length [6]. The fifth digit is zero and not always used. A disadvantage of Li-Ion batteries is in the extreme reactions in cases of abusive conditions, which include, among others, overcharging, high temperatures or separator cracking, due to excessive mechanical loads. Such conditions are associated with the danger of an internal short circuit and a possible thermal runaway. Liu et al. [7,8] studied this behavior in pouch cells where the temperature generated by a short circuit exceeded several hundred degrees Celsius, depending on the state of charge. Li et al. [9] investigated the mechanical behavior of 18650 cylindrical cells and 20 Ah pouch cells as a function of SoC. Soudbakhsh et al. [10] investigated the effect of mechanical damage on the electrical response of the 18650 cells. Gilaki et al. [11,12] investigated the behavior of single 18650 cells, as well as in the cell cluster. Kermani et al. [13] studied the mechanical behavior of pouch cells and 18650 cylindrical cells under axial loading. Based on these results, and the realization that the plastic separator plays a central role in the safety of the cells, Bulla and Kolupaev have investigated different numerical methods for the calculation of the mechanical stress and the subsequent plastic deformations [14]. Other mechanical tests were performed by Keshavarzi et al. [15] on pouch cells, where the mechanical properties obtained by three-point bending tests were used for the characterization of the properties in tension. Kisters et al. [16] performed tests on elliptic and pouch cells using a spherical impactor on dry and wet cells. Recent tests by Song et al. [17] on 18650 cells were performed under both axial and lateral loading cases, as well as three-point bending. Sahraei et al. [18] investigated three types of lithium-ion pouch cells where different shaped indenters were used, and found the correspondence of the onset of a short circuit with the peak load for each test. Separator failures have been categorized into two types, a soft short circuit, which is observed with a soft drop of force and voltage, and a slight increase in temperature, and a hard short, which leads to a steeper drop in the voltage and force with a possible thermal runaway, as explained by Zhang [19]. Due to these findings, and the important role that the separator plays during the onset of short circuit, Bulla et al. focused on studying the properties of the separator. Their research [20] focused on the investigation of the failure behavior of the separator material, and as a result, a new failure criterion, based on failure strain vs. the stress triaxiality, was developed and implemented in Altair Radioss [21]. Within this failure criterion, the dependency of the loading velocity was added, which resulted in the prediction of the mechanical response study of polyethylene (PE) separator materials. An additional physical effect was considered, which is the high orthotropic behavior of this material, due to its manufacturing processes. Within further investigations of the separator material, a new material model was developed based on the findings of these tests, which considers the visco-elasticity and visco-elasto-plasticity and orthotropic behavior of the separator material [22], used in 18650 cylindrical cells. A comparison between the widely-used 18650 vs. 21700 cells was provided by Quinn and Waldmann. Within their study, the design and capacity [23,24] of these two cell sizes were compared. As a result of this study, the 21700 Li-ion battery cell shows a 50% higher energy storage capacity compared to the 18650 cells. The increased generation of electrical power by photovoltaics, wind power, and other regenerative sources drives the development of batteries with increased efficiency. Additionally, an increase in the range with a single charge, which leads to an increase in the distance travelled, is a central development goal of the automotive industry. Customer demands for vehicles with a higher range, in

combination with legal requirements for climate protection by limiting CO_2 emissions, are the motivation for increasing the efficiency of electric vehicles. In addition to the ecological motivation, economic factors are a major incentive for vehicle manufacturers to focus on reducing the development time of their vehicles by using high-fidelity simulation tools, such as finite element analysis. To increase the battery performance of portable electronic devices, such as laptops or mobile phones, product development also benefits from higher accuracy of FEA results. To achieve this goal, more precise FE models are required to describe the mechanical behavior of Li-ion battery cells. This will allow an increase in the electric storage possibility, but not the weight of the protective systems of the battery casings.

In this study, for the first time, a commercial high capacity 21700 Li-Ion battery cell was investigated regarding its mechanical response under the different impact velocities of a flat impactor and different states of charge. Figure 1 shows the 21700 Li-ion battery, which is the subject of the present study.

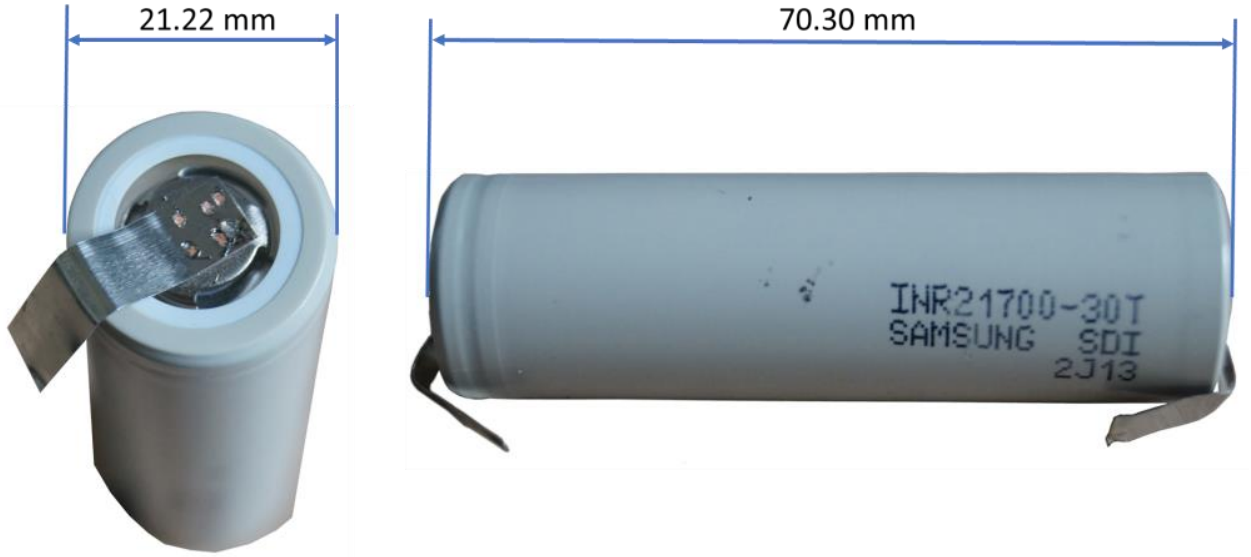

Figure 1. Samsung INR21700-30T Li-Ion cell, used within this study.

2. Materials and Methods

2.1. Test Preparation

Rechargeable Lithium-ion cells, produced by Samsung SDI Co., Ltd. Cell Business Division, were used for the experiments. The exact model name of the cells used is INR21700-30T. The cell weighs 70 g. The nominal voltage is 3.6 V. The cells have been mechanically tested by the manufacturer via a drop test from a height of 1.0 m in a random direction three times onto a concrete floor, according to the IEC62133 standard with a fully charged cell, and a vibration test, according to the UN38.3 standard. Figure 2 shows the x-ray scan performed within this study using one of these 21700 Li-ion cells, compared to a classic 18650 cell. It can be seen that, in addition to the overall size difference, the structure of the 21700 cells misses the metal tube mandril in the center (left hand side), which is present for the 18650 cell (right hand side). The usage of an inner tube only depends on the manufacturer. The center of the 21700 cell only shows the small copper connector plate, which can be also seen in the 18650 cell, Figure 3.

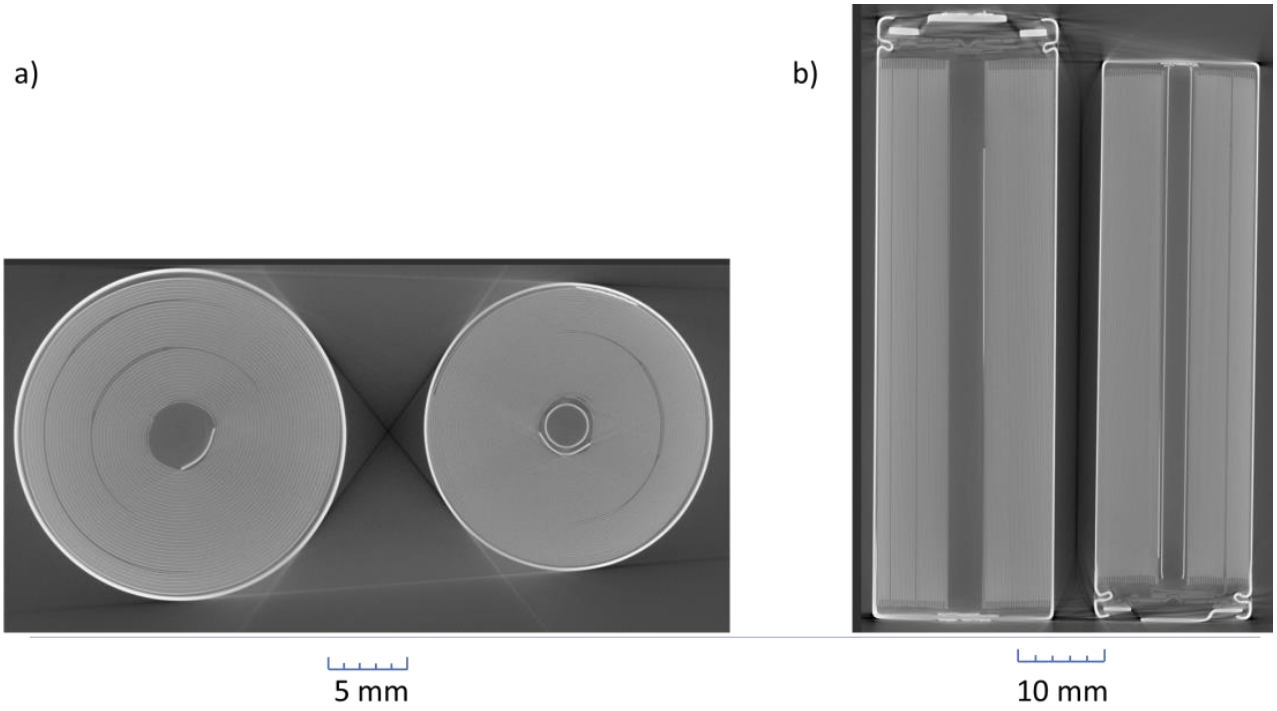

Figure 2. Comparison of X-ray photos of: (**a**) top-view of the in this study investigated 21700 (**left**) and 18650 (**right**) Li-ion cell. (**b**) front-view of 21700 Li-ion cell (**left**) and 18650 Li-ion cell (**right**).

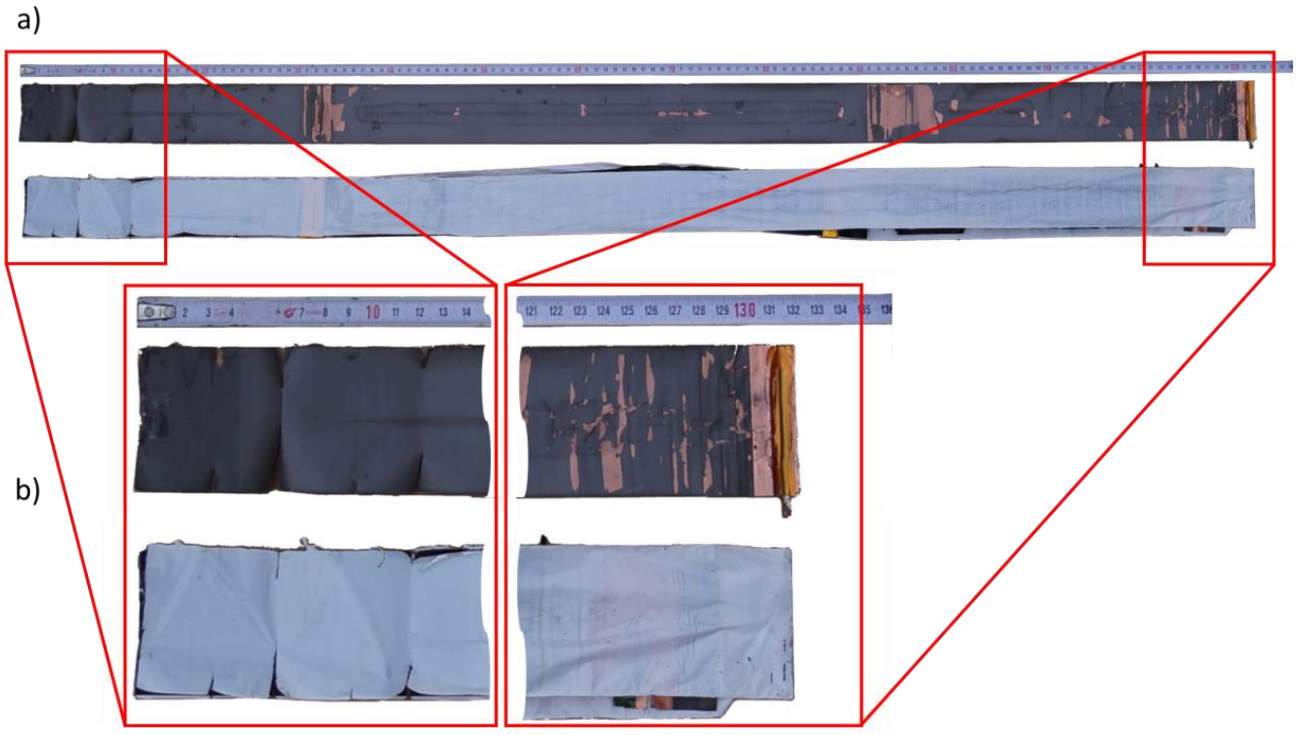

Figure 3. Disassembled cylindrical 21700 cell. Inner parts consist of anode, cathode, and separator. Showing the entire length (**a**) and zoomed view (**b**) at both ends.

After a cell was completely discarded, it was dissected, and the inner jellyroll was completely unwrapped (Figure 3). The total measured length of the individual components (copper, aluminum, and PE separator foils) is about 1320 mm. The width of the anode copper sheet is about 63.5 mm, and its thickness is 0.1 mm. The cathodic aluminum part has a width of about 61.7 mm and a of thickness about 0.1 mm. The width of the PE

separator is 65 mm and its thickness is about 20 µm, which is within the range of other Li-ion cells [25,26]. Figure 3 shows the thin and brittle coating layer.

Figure 4 shows the opened steel casing (a) and the thickness of the steel casing, scanned, and measured with X-rays before cutting and opening (b). The steel casing is made of a mild steel that is very easy to deep-draw. Neither the real measurement nor the optical X-ray measurement show any significant variation in thickness. Both measurements agree very well and show a constant of about 0.22 mm over the cell length.



Figure 4. Opened steel casing of the 21700 cell (**a**) and the X-ray scanned casing with optical measured casing thickness distribution over the cell length (**b**).

Before starting the mechanical testing, the cells were adjusted to the desired SoC. This procedure was performed in six steps:

1. The cells were delivered with a SoC of around 40–50%.
2. All cells were discharged to the cut-off voltage (0% SoC).
3. All cells were fully charged until full nominal capacity (100% SoC).
4. After these steps, two full cycles were carried out to bring the cells to the normal mode.
5. Then, a full discharge was performed until cut-off (0%).
6. Finally, the cells were charged to the specified SoC by measuring the input current, according to the test program.

During cycling, one can monitor whether the cells reach the nominal capacity or if there are any defects. There were no defects with these cells.

Table 1 shows the entire test-matrix. It can be seen from the table that the measurements of cell No. 13 were not consistent, so this cell was not considered for further post processing. Figure 5 shows the test set-up within the test chamber. During the test, the impactor velocity, reaction force, and voltage of the cell were measured. In addition to these values, a thermocouple was attached to each cell, which traced the temperature evolution during the test, directly on the cell. Another temperature measurement thermocouple element was used to measure the temperature within the chamber during the experiment.

Table 1. Test matrix.

Nr.	Sample Name	Velocity (mms^{-1})	SoC (%)	Remark
1	THM_V01#40%_C	10	40	ok
2	THM_V02#40%_C	10	40	ok
3	THM_V03#40%_C	10	40	ok
4	THM_V04#60%_C	10	60	ok
5	THM_V05#60%_C	10	60	ok
6	THM_V06#60%_C	10	60	ok
7	THM_V07#80%_C	10	80	ok
8	THM_V08#80%_C	10	80	ok
9	THM_V09#80%_C	10	80	ok
10	THM_V10#100%_C	10	100	ok
11	THM_V11#100%_C	10	100	ok
12	THM_V12#100%_C	10	100	ok
13	THM_V13#40%_C	100	40	not ok
14	THM_V14#40%_C	100	40	ok
15	THM_V15#40%_C	100	40	ok
16	THM_V16#60%_C	100	60	ok, but no temperature data
17	THM_V17#60%_C	100	60	ok
18	THM_V18#60%_C	100	60	ok
19	THM_V19#80%_C	100	80	ok
20	THM_V20#80%_C	100	80	ok
21	THM_V21#80%_C	100	80	ok
22	THM_V22#100%_C	100	100	ok
23	THM_V23#100%_C	100	100	ok
24	THM_V24#100%_C	100	100	ok
25	THM_V25#40%_C	1000	40	ok
26	THM_V26#40%_C	1000	40	ok
27	THM_V27#40%_C	1000	40	ok
28	THM_V28#60%_C	1000	60	ok
29	THM_V29#60%_C	1000	60	ok
30	THM_V30#60%_C	1000	60	ok
31	THM_V31#80%_C	1000	80	ok
32	THM_V32#80%_C	1000	80	ok
33	THM_V33#80%_C	1000	80	ok
34	THM_V34#100%_C	1000	100	ok
35	THM_V35#100%_C	1000	100	ok
36	THM_V36#100%_C	1000	100	ok

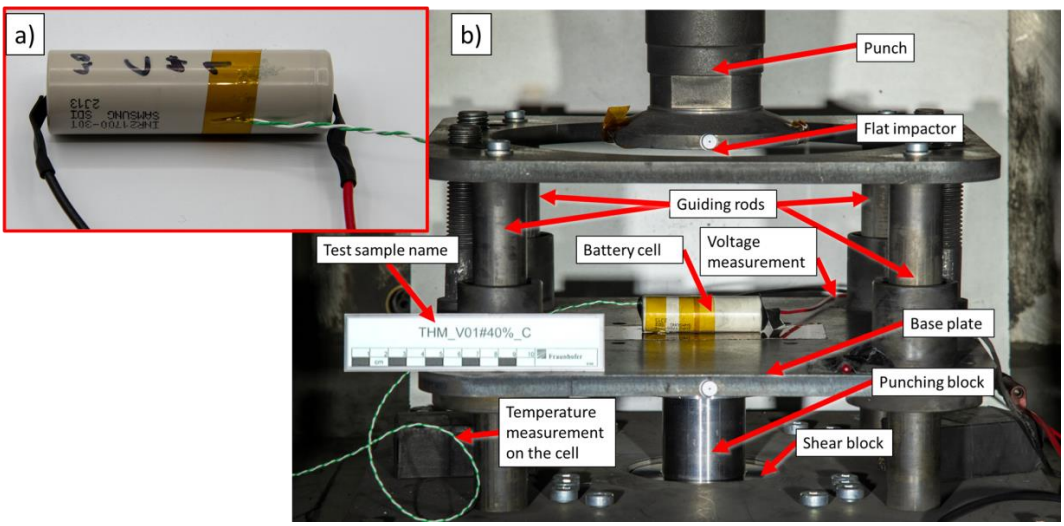

Figure 5. Experimental setup of 21700 battery cell (**a**), in the test chamber (**b**).

2.2. Test Results

The tests were carried out at the Fraunhofer Institute EMI [27], in a closed test chamber with an exhaust system to avoid the escape of noxious fumes.

Figure 5 shows the test set-up in the test chamber, with the mounted flat impactor underneath the punch. All tests were performed at a constant velocity, according to the test matrix. At the lowest velocities, the maximum displacement is 11 mm. For higher test velocities, the stop criterion is set to a maximum force of 300 kN, at which the shear block below the battery plate fractures and is knocked out. This is a safety measure to prevent damage to the test rig.

The resultant displacements can vary at higher impactor velocities. For some, the displacement is up to 17 mm. Figure 6 shows the experimental test #1, in sequence with the 40% SoC battery cell and an impact velocity of 10 mms^{-1}.

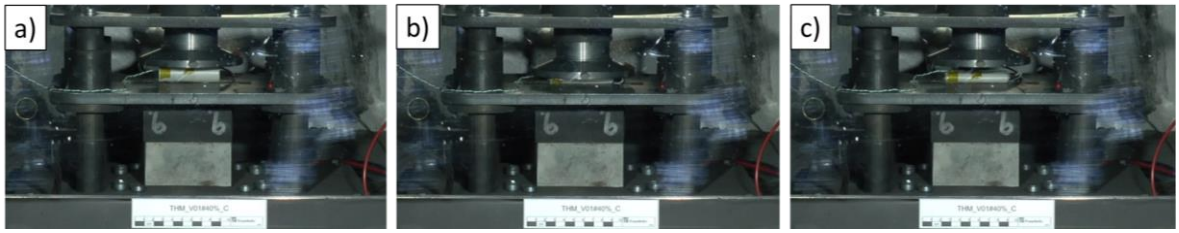

Figure 6. Experiment: Flat compression with v = 10 mms^{-1} of cell with SoC of 40%. (**a**) first contact between flat impactor and batterie. (**b**) maximum intrusion and (**c**) end of test, impactor is moving upward.

No visible thermal runaway or sparkles were observed at any of the three tests with the SoC of 40%. The temperature measured by the thermocouple mounted directly on the cell shows an increase in the posttest temperature, up to 70 °C after ~1 min. The measured temperature inside the test chamber does not show any increase up to ~2 min posttest. Figure 7 shows the experimental test sequence of test #4, with the 60% SoC battery and an impact velocity of 10 mms^{-1}. The first visible thermal runaway cases were observed in two of the three tests at 60% SOC, after reaching the maximum intrusion. After first contact (a) and the progress of compaction to the maximum displacement (b), the first exhausts and sparkles, up to visible flames and fire, were visible in these tests. The temperature measured directly from the cells reached ~260 °C in 5 of 9 tests (see Table 1) performed at this SOC.

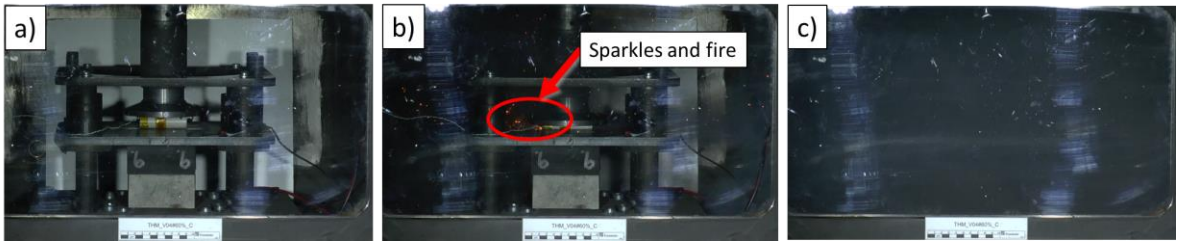

Figure 7. Experiment: Flat compression with v = 10 mms^{-1} of cell with SoC of 60%. (**a**) first contact between flat impactor and batteries. (**b**) maximum intrusion and (**c**) end of test, impactor is moving upward.

Figure 8 shows the flat compression tests of the battery cells with 80% SoC. Early fire and an extreme thermal reaction up to explosion is observed in two of the three tests. The temperatures measured at the cells were over 300 °C. In two cases, the temperature exceeded 500 °C. All battery cells with a SoC of 100% show the thermal runaway and extreme thermal reactions.

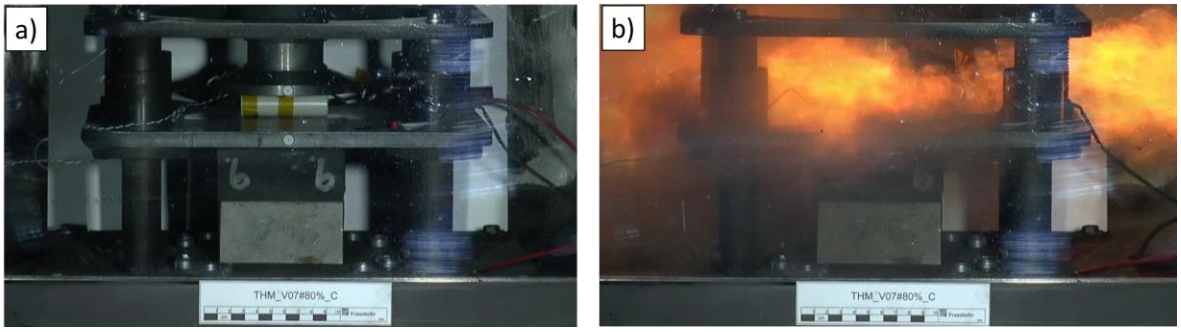

Figure 8. Experiment: Flat compression with v = 10 mms^{-1} of cell with SoC of 80%. (**a**) first contact between flat impactor and batteries. (**b**) maximum shows maximum intrusion and the fire burst.

Figure 9 shows the evolution of the temperature versus the time measured with a thermocouple mounted on the cell. The SoC is (Figure 9a) 60% and (Figure 9b) 100%, and the loading velocity is set at 10 mms^{-1}. The maximum temperature measured during the entire study is around 1100 °C in test No. 11. The temperature measurements show a large scatter range in all tests. Measuring cell temperatures at higher speeds is difficult and sometimes not useful, because the cells are destroyed before the thermocouple can register the temperature change. The measurements of the temperatures inside the chamber also show a large scatter, since the direction of the flames emerging from the cells is undefined and in some cases are directed straight at the thermocouple in the test chamber.

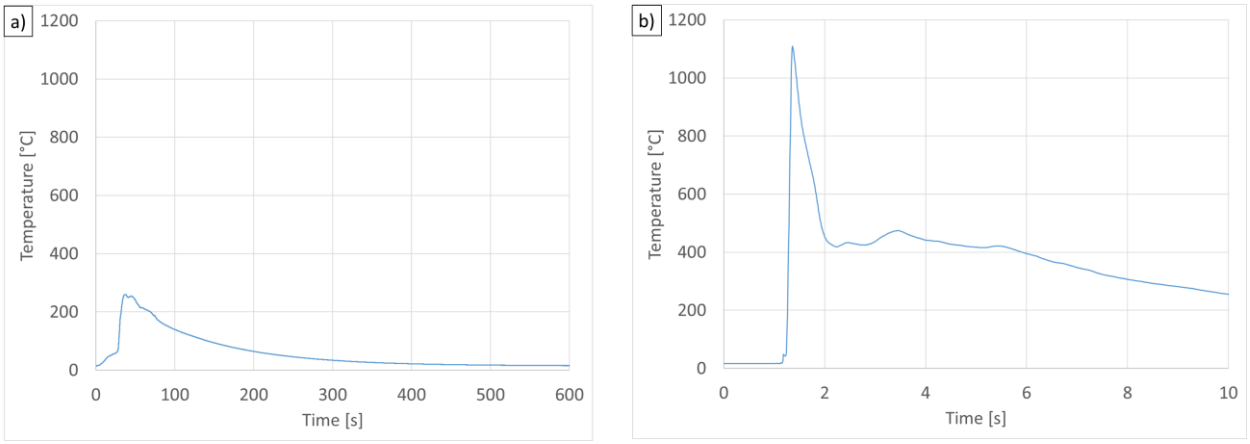

Figure 9. Measured temperature vs. time of the cell test (**a**) no 4 with a SOC of 60% and (**b**) No. 11 with a SoC of 100%.

Figure 10 shows the influence of the SoC measured with an impact velocity of 10 mms^{-1}. As the SoC increases, the maximum force achieved also increases from a minimum value of about 90 kN at a SoC level of 40%, to 110 kN at a SoC level of 100%. The stiffness does not vary in a larger range with the different SoCs. A possible explanation for an increasing force with a higher SoC could be a volumetric intrinsic strain, caused by the ion transport. Regarding the design of the cylindric cells, the dilatation is constrained due to the presence of the steel casing, which leads to an internal, mechanical pre-stressed condition. The higher the SoC, the higher the volumetric dilatation is. This is not observed regarding pouch cells, where the volume change is not comparably constrained. This effect is more thoroughly investigated by Li et al. [9].

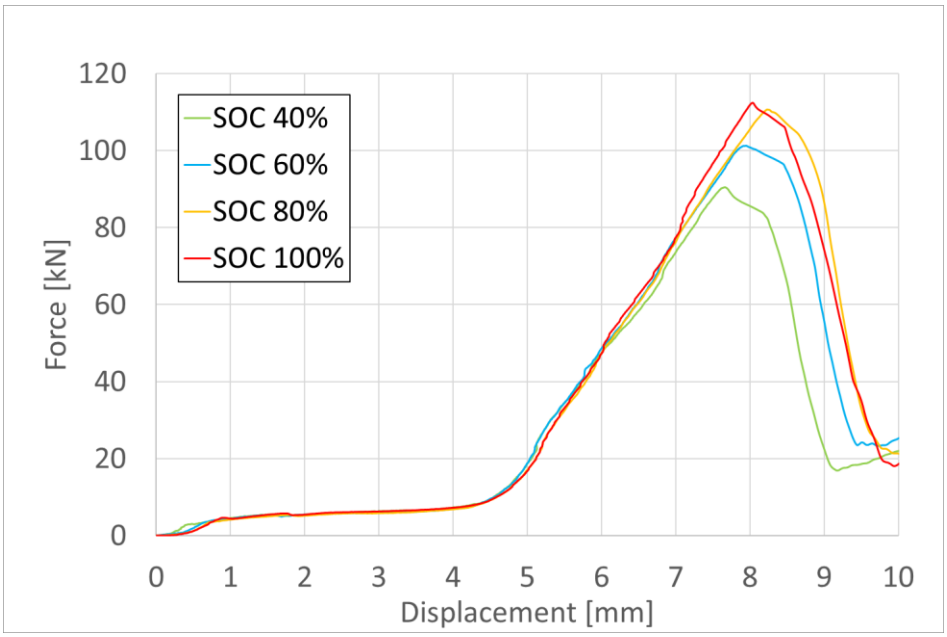

Figure 10. Force vs. displacement curves of experiments with different SoC at v = 10 mms^{-1}.

Figure 11 shows the influence of the three different impact velocities, and SoC of 40% (Figure 11a) and SoC of 100% (Figure 11b). Within the range of the results of these tests, there is no clear dependency of the impact velocity on the resultant force.

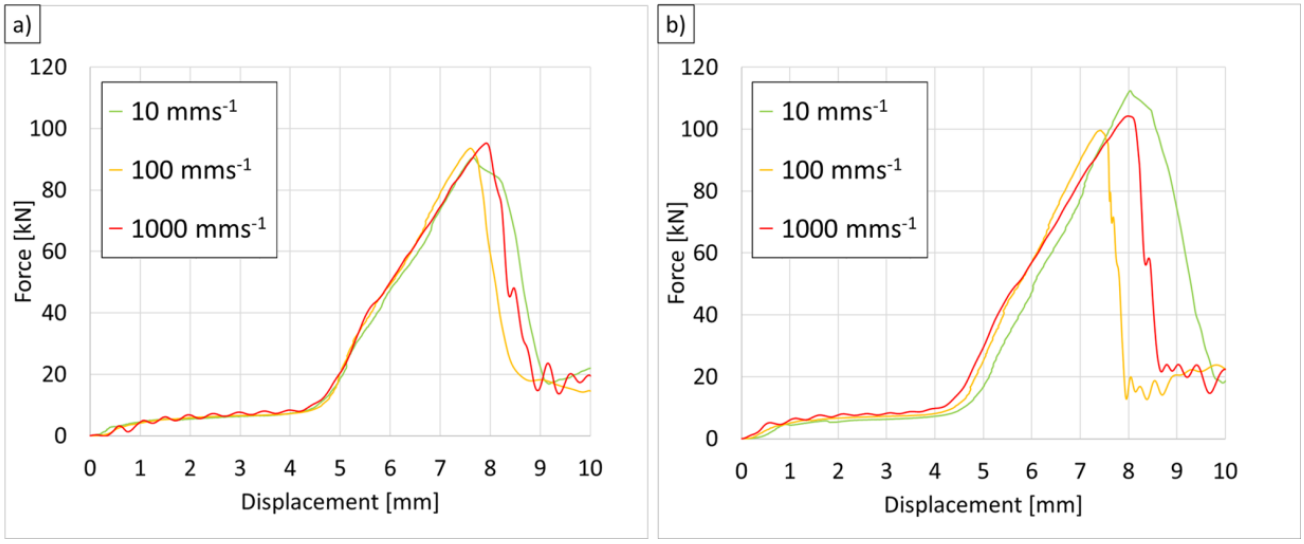

Figure 11. Force vs. displacement curves of experiments with different impact velocities and (**a**) 40% SoC and (**b**) 100% SoC.

Figure 12 shows the influence of voltage on the displacement of different SoC stages at an impact velocity of 10 mms^{-1}. The onset of a short circuit is detected at around an 8 mm displacement of the flat impactor. In some cases, an early and brief voltage drop was measured at between a 3 to 4 mm displacement, which quickly recovers to its initial value before the final voltage drop occurs.

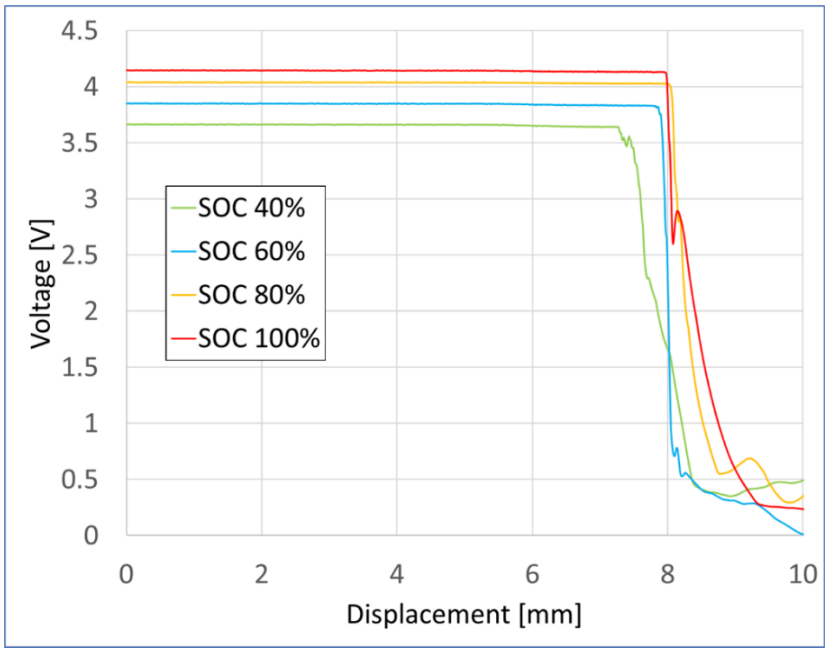

Figure 12. Voltage vs. displacement curves of experiments with different SoC at v = 10 mms^{-1}.

Figure 13 shows the influence of the onset of the short circuit, measured by the voltage drop as a function of the impactor velocity and the state of charge (a) at 40% and (b) at 100%.

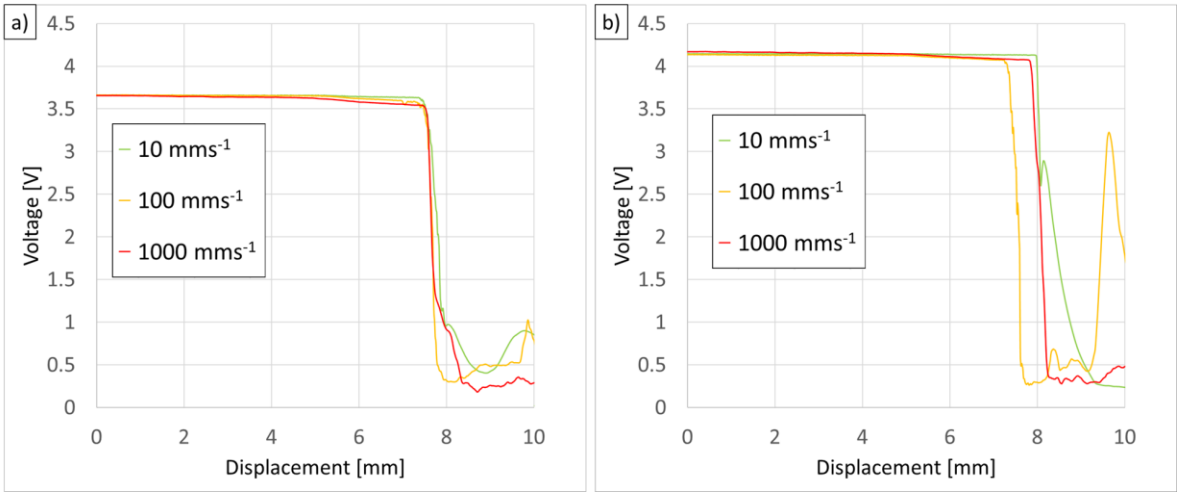

Figure 13. Voltage vs. displacement curves of experiments with different impact velocities and (**a**) 40% SoC and (**b**) 100% SoC.

A lager scatter of results is observed during the experiments. The figures represent a typical measurement curve of a specific test setup.

3. Modeling and Results

In order to develop a method for a FEM (finite element method) analysis, a model is created; this is able to predict the mechanical behavior of the tested Li-ion 21700 cells. The pre-processor HyperWorks (version 2022) by Altair Engineering Inc. (1820 E. Big Beaver Rd., Troy MI 48083, USA) is used on a Windows64 computer, using four Intel i7-6820 CPUs at 2.7 GHz with 32 GB RAM. Based on the results of the material tests, a novel material model for finite element analysis is developed using the explicit solver OpenRadioss [28].

FEM Model

Figure 14a shows the entire FEM model of the li-ion 21700 cell. It consisted of 20782 nodes and 5824 4-node-shell elements to model the steel casing and the closing plate. Additionally, 12800 solid (hexahedron) elements were used to model the jellyroll at its macroscopic level. The average element length was around 1 mm. The interaction between the three parts was realized by a penalty contact interface. The loading was applied by two rigid infinite-size planar walls. The lower one was fixed in space, whereas the upper one was moving in a z-direction towards the lower one with a constant velocity. All other boundary conditions were fixed. A static friction coefficient of 0.2 was applied to the rigid wall contact treatment. An All-vs-All penalty contact interface was used to model the internal contact between all parts of the battery cell. After a 10 mm displacement of the upper rigid wall, the simulation reaches its end and the run stops.

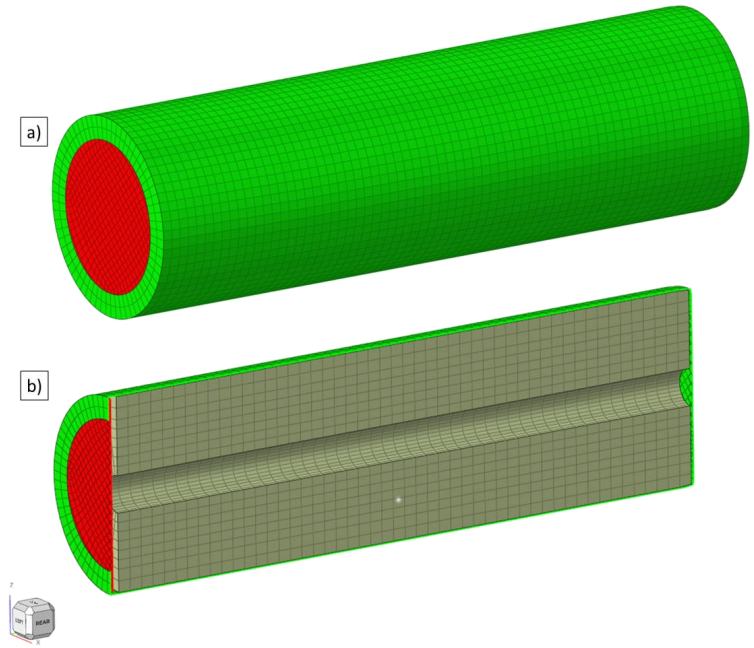

Figure 14. Entire FEM model (**a**), and vertical section cut (**b**).

Based on the measured constant thickness along the entire length of the battery casing and the ease of the cutting process, a highly ductile and well formable mild steel was assumed for the shell casing. Therefore, the material properties of a DC03 to DC04 grade material was used for the simulation model with a Youngs modulus of 210 GPa, Poisson's ratio of 0.3, yield stress of 0.15 GPa, ultimate stress of 0.38 Gpa, and strain at ultimate stress of 0.24. A material model, to model the nonlinear mechanical behavior of the steel casing of an elasto-plastic material model, based on Johnson-Cook equation [29], was used to describe the mechanical behavior of mild steel; this used the true stress vs. true strain curves in the plastic domain:

$$\sigma_{yield} = A + B\bar{\varepsilon}_{pl.}{}^{n} \quad (1)$$

where:

σ_{yield} = yield stress [GPa],
$\bar{\varepsilon}_{pl.}$ = equivalent plastic strain [-],
A = Hardening coefficient [GPa],
n= Hardening exponent [-],
With the values of A = 0.15, B = 0.521634 and n = 0.31557.

A viscoelastic foam material model was chosen as the material model for the jellyroll, which requires a tabulated input to describe the hardening behavior, as shown in Figure 15. The values of the curve are obtained by an iterative optimization procedure. The density was calculated to a value of 2.695 kg/mm^3. Depending on the mesh size used, a fracture

criterion is applied; this deletes elements after reaching a strain of 0.34 in the 1st principal direction by adding an additional failure criterion to the material definition used.

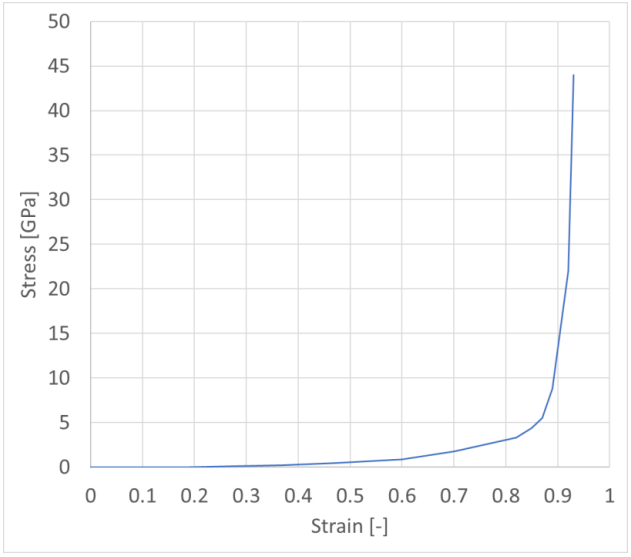

Figure 15. Stress vs. strain curve used to model the jellyroll material behavior.

For post-processing, the reaction forces and the displacement of the rigid wall are tracked and stored in the time history results file.

Figure 16 shows the comparison between the measured force-displacement behavior of the real test (black curve) and the FEM simulation (red curve).

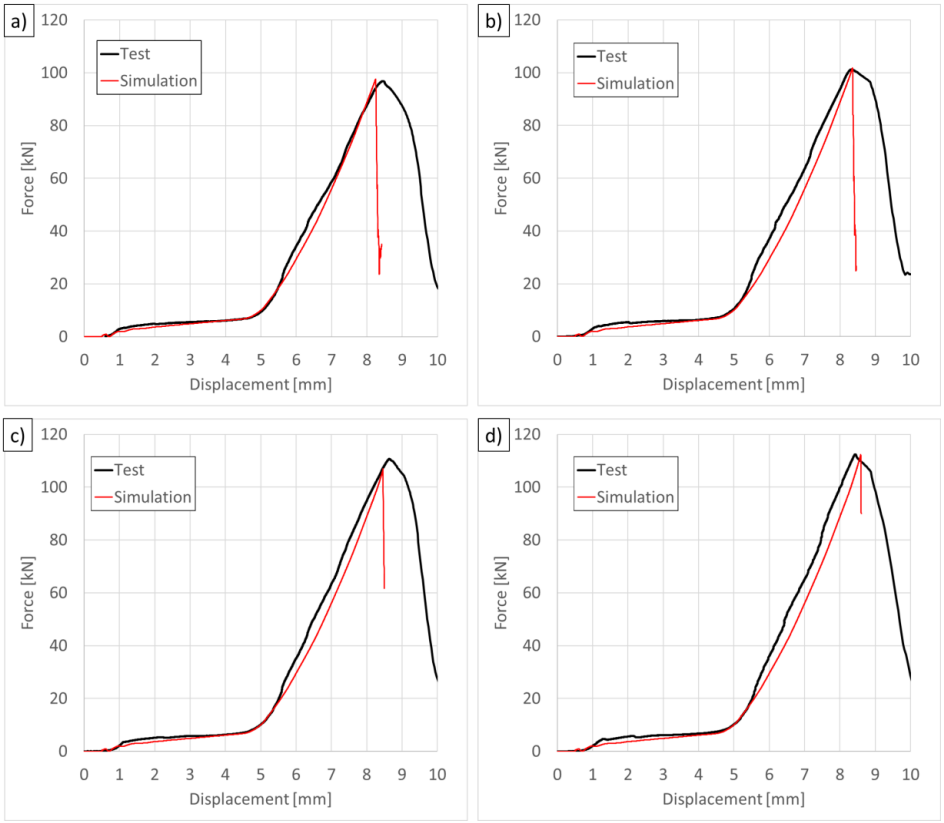

Figure 16. Force vs. displacement chart showing test vs. simulation curves at v = 10 mms^{-1} and (**a**) 40% SoC, (**b**) 60% SoC, (**c**) 80% SoC, and (**d**) 100% SoC.

The increment of increased failure strain is set to 0.006 [-] to model the different failure force.

Figure 17 shows the comparison between the deformed Li-ion 21700 cell in the experiment (a) and the FEM model (b).

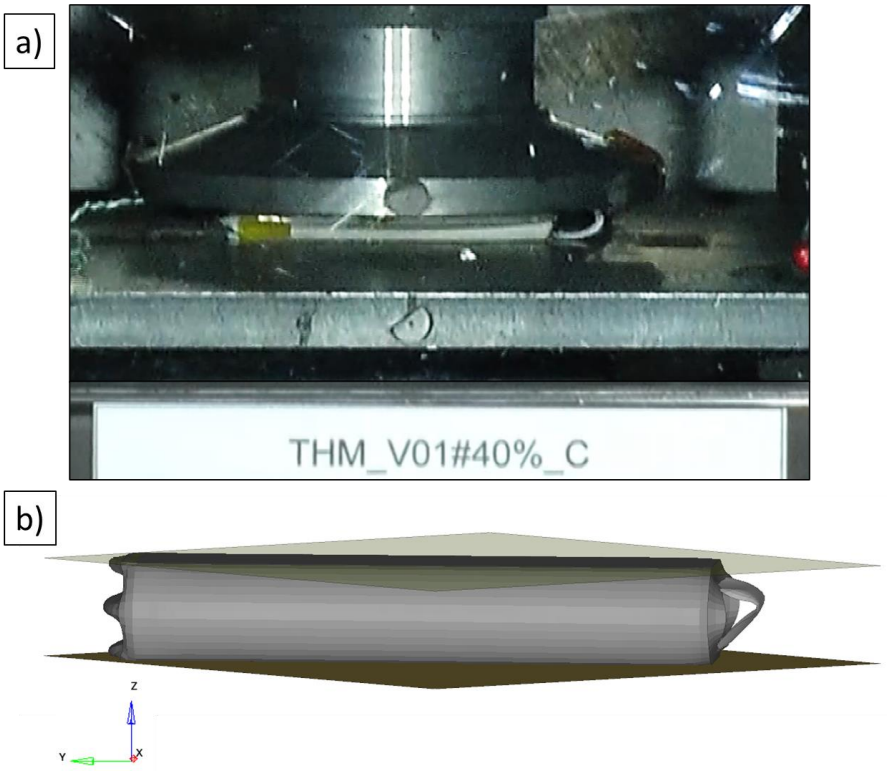

Figure 17. Deformed cell (**a**) and the corresponding FEM model (**b**).

Simulations were performed using the explicit FEA solver OpenRadioss on a Windows64 computer with four Intel i7-6820 CPUs at 2.7 GHz with 64 GB RAM. OpenRadioss solves the entire simulation with 230,000 cycles and an average timestep of 1×10^{-5} to 5×10^{-5} ms. The simulation duration on a Microsoft Windows64 computer using four Intel i7-6820 CPUs at 2.7 GHz with 32 GB RAM was approximately 10 min.

4. Discussion

The objective of the present work was to perform real-life mechanical, flat compression tests of Li-ion 21700 cells under high mechanical loads with different loading velocities and different states of charge in the cells. The aim was to develop a FEA model that is capable of predicting the mechanical behavior observed in the experiments. As observed in the tests, the onset of a short circuit, followed by a thermal runaway, occurs in cells with a SoC of 60% and above. Nevertheless, a large scatter is observed in the tests results. The observed voltage drop corresponds with the maximum force level measured in the test. Therefore, the focus of the current work is to accurately predict the force-displacement behavior in FEA compared to the experiment; this is in order to predict the risk of thermal runaway, fire, and explosion. This is achieved by using a homogenized approach and determining the appropriate material parameter.

In future work, an improved material model will be used to more accurately predict the area of a possible internal short circuit; this might lead to the risk of thermal runaway, depending on the battery cell SoC, as well as the entire cell pack. In this work, an isotropic material model and a simplified failure criterion were used to predict the behavior of the jellyroll. Since the separator plays an important role in the occurrence of a short

circuit, further investigation of its behavior is ongoing. Further research will require the development of a more advanced material model.

5. Conclusions and Outlook

In this study, a new FEA model is developed; it accurately predicts the force versus displacement behavior of the high-capacity Li-Ion 21700 cells, based on experimental results.

As observed in the experiments, high mechanical loads on charged Li-ion cells can lead to thermal runaway with disastrous consequences. Therefore, a qualitative and quantitative prediction of high loading in different load cases is crucial to design countermeasures and protective structures in the right locations, without adding too much mass to the entire system. Further developments are ongoing to consider the influence of the SoC on material stiffness and damage. The FEM model developed in this work is capable of predicting the mechanical response very accurately and can be used directly in the open-source solver OpenRadioss; therefore, it will be available for applications in e-mobility, as well as in consumer products in the near future.

Author Contributions: Conceptualization, M.B., S.K., E.S. and T.K.; Formal analysis, S.K.; Methodology, M.B. and E.S.; Resources, T.K., S.K. and E.S.; Software, M.B.; Supervision, S.K. and E.S.; Validation, M.B., S.K., E.S. and C.S.; Visualization, M.B.; Writing—original draft, M.B. All authors have read and agreed to the published version of the manuscript.

Funding: This research received no external funding.

Institutional Review Board Statement: Not applicable.

Informed Consent Statement: Not applicable.

Data Availability Statement: Not applicable.

Conflicts of Interest: The authors declare no conflict of interest.

References

1. Viebahn, P.; Nitsch, J.; Fischedick, M.; Esken, A.; Schuewer, D.; Supersberger, N.; Zuberbuehler, U.; Edenhofer, O. Comparison of carbon capture and storage with renewable energy technologies regarding structural, economic, and ecological aspects in Germany. *Int. J. Greenh. Gas Control* **2007**, *1*, 121–133. [CrossRef]
2. Wei, Z.; Zou, C.; Leng, F.; Soong, B.H.; Tseng, K.-J. Online Model Identification and State-of-Charge Estimate for Lithium-Ion Battery with a Recursive Total Least Squares-Based Observer. *IEEE Trans. Ind. Electron.* **2018**, *65*, 1336–1346. [CrossRef]
3. Lithium-Ion-Batteries. Available online: https://www.akkuparts24.de/Lithium-Ion-batteries (accessed on 17 August 2022).
4. Battery Types Explained. Available online: https://blog.teufelaudio.com/battery-types/ (accessed on 22 September 2022).
5. Canals Casals, L.; Macarulla, M.; Gómez-Núñez, A. High-Capacity Cells and Batteries for Electric Vehicles. *Energies* **2021**, *14*, 7799. [CrossRef]
6. Lithium-Ionen-Akkumulator. Available online: https://de.wikipedia.org/wiki/Lithium-Ionen-Akkumulator (accessed on 22 September 2022).
7. Liu, Y.; Li, Y.; Liao, Y.G.; Lai, M.-C. Effects of State-of-Charge and Penetration Location on Variations in Temperature and Terminal Voltage of a Lithium-Ion Battery Cell during Penetration Tests. *Batteries* **2021**, *7*, 81. [CrossRef]
8. Feng, X.; Sun, J.; Ouyang, M.; Wang, F.; He, X.; Lu, L.; Peng, H. Characterization of penetration induced thermal runaway 346 propagation process within a large format lithium ion battery module. *J. Power Sources* **2015**, *275*, 261–347, +273. [CrossRef]
9. Li, W.; Xia, Y.; Zhu, J.; Luo, H. State-of-Charge Dependance of Mechanical Response of Lithium-Ion Batteries: A Result of Internal Stress. *J. Electrochem. Soc.* **2018**, *165*, A1537. [CrossRef]
10. Soudbakhsh, D.; Gilaki, M.; Lynch, W.; Zhang, P.; Choi, T.; Sahraei, E. Electrical Response of Mechanically Damaged Lithium-Ion Batteries. *Energies* **2020**, *13*, 4284. [CrossRef]
11. Gilaki, M.; Song, Y.; Sahraei, E. Homogenized characterization of cylindrical Li-ion battery cells using elliptical approximation. *Int. J. Energy Res.* **2021**, *46*, 5908–5923. [CrossRef]
12. Gilaki, M.; Walsh, R.; Sahraei, E. Model-Based Design of an Electric Bus Lithium-Ion Battery Pack. *ASME J. Electrochem. Energy Conv. Stor.* **2021**, *18*, 020914. [CrossRef]
13. Kermani, G.; Keshavarzi, M.; Sahraei, E. Deformation of lithium-ion batteries under axial loading: Analytical model and Representative Element. *Energy Rep.* **2021**, *7*, 2849–2861. [CrossRef]
14. Bulla, M.; Kolupaev, V. Stress Analysis in Design with Plastics: Accessible Method with huge Impact. *J. Polym. Mater.* **2021**, *74*, 60–67.

15. Keshavarzi, M.; Gilaki, M.; Sahraei, E. Characterization of in-situ material properties of pouch lithium-ion batteries in tension from three-point bending tests. *Int. J. Mech. Sources* **2022**, *219*, 107090. [CrossRef]
16. Kisters, T.; Gilaki, M.; Nau, S.; Sahraei, E. Modeling of Dynamic Mechanical Response of Li-Ion cells with Homogenized Electrolyte-Solid Interactions. *J. Energy Storage* **2022**, *49*, 104069. [CrossRef]
17. Song, Y.; Gilaki, M.; Keshavarzi, M.; Sahraei, E. A universal anisotropic model for a lithium-ion cylindrical cell validated under axial, lateral, and bending loads. *Energy Sci. Eng.* **2022**, *10*, 1431–1448. [CrossRef]
18. Sahraei, E.; Meier, J.; Wierzbicki, T. Characterizing and modeling mechanical properties and onset of short circuit for three types of lithium-ion pouch cells. *J. Power Sources* **2014**, *247*, 503–516. [CrossRef]
19. Zhang, X.; Sahraei, E.; Kai, W. Deformation and failure characteristics of four types of lithium-ion battery separators. *J. Power Sources* **2016**, *327*, 693–791. [CrossRef]
20. Bulla, M.; Kolling, S.; Sahraei, E. An Experimental and Computational Study on the Orthotropic Failure of Separators for Lithium-Ion Batteries. *Energies* **2020**, *13*, 4399. [CrossRef]
21. Altair Engineering, Inc. RADIOSS Manual, USA. 2022. Available online: www.altairhyperworks.com (accessed on 17 March 2020).
22. Bulla, M.; Kolling, S.; Sahraei, E. A Material Model for the Orthotropic and Viscous Behavior of Separators in Lithium-Ion Batteries under High Mechanical Loads. *Energies* **2021**, *14*, 4585. [CrossRef]
23. Quinn, J.B.; Waldmann, T.; Richter, K.; Kasper, M.; Wohlfahrt-Mehrens, M. Energy Density of Cylindrical Li-Ion Cells: A Comparison of Commercial 18650 to the 21700 Cells. *J. Electrochem. Soc.* **2018**, *165*, A3284–A3291. [CrossRef]
24. Waldmann, T.; Scurtu, R.-G.; Richter, K.; Wohlfahrt-Mehrens, M. 18650 vs. 21700 Li-ion cells—A direct comparison of electrochemical, thermal, and geometrical properties. *J. Power Sources* **2020**, *472*, 228614. [CrossRef]
25. Sahraei, E.; Hill, R.; Wierzbicki, T. Calibration and finite element simulation of pouch lithium-ion batteries for mechanical integrity. *J. Power Sources* **2012**, *201*, 307–321. [CrossRef]
26. Sahraei, E.; Bosco, E.; Dixon, B.; Lai, B. Microscale failure mechanisms leading to internal short circuit in Li-ion batteries under complex loading scenarios. *J. Power Sources* **2016**, *319*, 56–65. [CrossRef]
27. Kotter, P.; Kisters, T.; Schleicher, A. Dynamic impact tests to characterize the crashworthiness of large-format lithium-ion cells. *J. Energy Storage* **2019**, *26*, 100948. [CrossRef]
28. OpenRadioss. Available online: https://www.openradioss.org (accessed on 17 September 2022).
29. Johnson, G.R.; Cook, W.H. A Constitutive Model and Data for Metals Subjected to Large Strains, High Strain Rates and High Temperatures. In Proceedings of the 7th International Symposium on Ballistics, Hague, The Netherlands, 21 April 1983.

Disclaimer/Publisher's Note: The statements, opinions and data contained in all publications are solely those of the individual author(s) and contributor(s) and not of MDPI and/or the editor(s). MDPI and/or the editor(s) disclaim responsibility for any injury to people or property resulting from any ideas, methods, instructions or products referred to in the content.